Colloids and Surfaces A: Physicochem. Eng. Aspects 345 (2009) 135–140

Contents lists available at ScienceDirect

Colloids and Surfaces A: Physicochemical and Engineering Aspects

journal homepage: www.elsevier.com/locate/colsurfa

Nickel (II) sorption on porous ZnO prepared by solution combustion method

Y. Alvarado-Ibarra[a,b], F. Granados-Correa[a,*], V.H. Lara[c], P. Bosch[d], S. Bulbulian[e]

[a] Instituto Nacional de Investigaciones Nucleares, Departamento de Química, A. P. 18-1027, Col. Escandón, Delegación Miguel Hidalgo, C.P. 11801 México D.F., México
[b] Instituto Tecnológico de Toluca, Av. Instituto Tecnológico S/N. Ex Rancho La Virgen, Metepec, Estado de México, México
[c] Universidad Autónoma Metropolitana, Iztapalapa, A. P. 55-532, Av. San Rafael Atlixco No. 186, Col. Vicentina, C.P. 09340 México D.F., México
[d] Instituto de Investigaciones en Materiales, Universidad Nacional Autónoma de México, A.P. 70-360, C.P. 0451 México D.F., México
[e] Centro de Ciencias Aplicadas y Desarrollo Tecnológico, Universidad Nacional Autónoma de México, A.P. 70-186, C.P. 04510 México D.F., México

ARTICLE INFO

Article history:
Received 13 February 2009
Received in revised form 21 April 2009
Accepted 23 April 2009
Available online 3 May 2009

Keywords:
Zinc oxide
Solution combustion method
Small angle X-ray scattering
Nickel sorption

ABSTRACT

Water effect on the combustion preparation of ZnO is presented. The obtained materials were characterized through their specific surface area, morphology, particle shape and fractal dimension. They were tested in Ni^{2+} sorption. The surface fractal dimension of the combustion prepared sample was 1.9 but in those where water was included it decreased to 1.8. In the sample prepared by calcination it was 2.1. A linear correlation between the fractal dimension and Ni^{2+} sorption was found.

1. Introduction

Powder substances have unique physical and chemical properties, which make them extremely good adsorbents. At the surface of these materials many wastewater ingredients can be retained. A wide variety of materials and manufacturing techniques are to produce them [1–6]. In this work, we focus our interest on inorganic oxide powders that possess some adsorption properties, among them one is zinc oxide. Zinc oxide adopts zincite structure which has a very high lattice energy (4033.4 kJ/mol). Zincite is a compound that may be synthesized by solid–vapor sublimation, precipitation or sol–gel methods [7–9].

The zinc oxide/carbon composite and the rapid combustion synthesis of ZnO using glycine as fuel have been already published [10–12]. Combustion synthesis technique requires the use of an organic compound, like urea, which, reacts with oxygen. In this sense, it is economical and fast, but it may issue in new morphologies or even different compounds than those provided by conventional precipitation [13]. However, the synthesis of pure ZnO by the solution combustion method using urea as fuel and zinc nitrate as oxidant has not been reported.

Solution combustion synthesis has been already used to produce oxides with large surface areas [14]. In a previous study, magnesium oxide was prepared by solution combustion and the cobalt sorption of these materials was discussed [15].

Still, in combustion methods using urea, the control of the very exothermal urea reaction with oxygen is crucial. Indeed, thermal gradients and gas fluxes shape particle morphology. For instance, combustion prepared materials with a hierarchical texture, as SiO_2 [16,17] or Al_2O_3 [18], present nanopores which are determining in their applications. Surface area or pore size distributions are, with morphology, some of the parameters that condition reactivity, electrochemical activities, or molecular sieve effect. As the main differences between conventionally synthesized oxides and combustion prepared materials are textural, their surface adsorption properties have to be different.

Nickel is a metal frequently encountered in raw wastewater streams from industries such as mining and metallurgy of nickel. Stainless steel, nickel electroplating, battery and accumulator manufacturing, pigment and ceramic industries produce wastewaters that contain high amounts of nickel (II) ions [19]. Nickel is also present in nuclear wastes due to its use in actinide research.

This metal is a corrosion product from cooling water systems in nuclear power plants as it may enter into the core, become activated, leading to activity build-up on the surface of the primary system. The system and the components turn out to be contaminated. Therefore, system decontamination is an important factor in reducing the radiation levels in a nuclear power plant [20].

In this work we present the solution combustion synthesis of ZnO and we compare the morphology of the obtained compounds varying several synthesis parameters with the corresponding sample synthesized by calcination of zinc nitrate. To test these surface structure variations, the nickel sorption, often found in wastewaters

* Corresponding author. Tel.: +55 53297200; fax: +55 53297301.
E-mail address: francisco.granados@inin.gob.mx (F. Granados-Correa).

0927-7757/$ – see front matter © 2009 Elsevier B.V. All rights reserved.
doi:10.1016/j.colsurfa.2009.04.045

from nuclear industry as nickel (II), is used. Indeed, nickel retention is, now, well understood [21,22].

2. Experimental

2.1. Materials

The following analytic grade materials were used without further purification: Urea NH_2CONH_2 A.C.S. reagent (Sigma–Aldrich, 99–100% wt purity), zinc nitrate hexahydrate $Zn(NO_3)_2{\cdot}6H_2O$ A.C.S. reagent (Sigma–Aldrich, 99% wt purity), nickel nitrate hexahydrate $Ni(NO_3)_2{\cdot}6H_2O$ reagent (Baker, 100.7% wt purity) and potassium bromide KBr (Madison Co. spectroscopy grade).

2.2. Synthesis of zinc oxide by calcination method

ZnO (sample A_{cal}) was prepared by calcination. 0.2 g of $Zn(NO_3)_2{\cdot}6H_2O$ was transferred into a 30 mL crucible, which was introduced for two hours into a muffle furnace. Heating temperature was 800 °C.

2.3. Synthesis of zinc oxide by combustion and solution combustion methods

Zinc oxide powder (sample B_{comb}) was prepared by combustion method, the best molar ratio was found to be with 0.2 g of $Zn(NO_3)_2$ $6H_2O$ and 0.4 g of urea mixed and suspended in 1 mL of distilled water until a homogeneous solution was obtained. The mixture was heated until most water evaporated with the help of an electric grill, resulting in a humid integrated solid.

Two more samples were prepared by solution combustion method, *i.e.*, diluting the humid integrated solid in additional 0.5 or 1 mL of distilled water (sample C_{scomb} and D_{scomb}), respectively. These mixtures were transferred into 30 mL crucibles which were introduced for five minutes into a muffle furnace. It was found that the best heating temperature to obtain ZnO was 800 °C. The essential difference between combustion and solution combustion methods was that, in the combustion synthesis the sample introduced in the furnace was dried until most water was evaporated whereas the two samples synthesized by the solution combustion procedure were wet.

2.4. Characterization

A Siemens D-5000 diffractometer coupled to a copper anode tube was used to obtain the X-ray diffraction patterns and identify the crystalline compounds. The K_α wavelength was selected with a diffracted beam monochromator.

To be sure that no organic radicals due to urea combustion remained, infrared experiments were performed. A spectrophotometer Nicolet 550 was used and the samples were mixed to KBr in the conventional way.

A Kratky camera coupled to a copper anode tube was used to measure the small angle X-ray scattering (SAXS) curves. The distance between the sample and the linear proportional counter was 25 cm; a Ni filter selected the copper K_α radiation. The sample was introduced into a capillary tube. Intensity $I(h)$ was measured for 9 min in order to obtain good quality statistics. The SAXS data were processed with the ITP program [23,24] where the angular parameter (h) is defined as $h = 2\pi\sin\theta/\lambda$, where θ and λ are the X-ray scattering angle and the wavelength, respectively. The shape of the scattering objects was estimated from the Kratky plot, *i.e.*, $h^2\ I(h)$ versus h. The shape is determined depending on the Kratky curve shape, then, for instance, if the curve presents a peak the particles are globular (bubbles) [25]. If a shape can be assumed, the size distribution function may be calculated. Finally, it is often useful to estimate, from the slope of the curve Log $I(h)$ versus Log(h), the fractal dimension of the scattering objects [26,27]. For this study the background obtained with the Porod plot was removed from the experimental intensity. The h interval was $0.07 < h < 0.18\ \text{Å}^{-1}$. Note that, by the Babinet principle, the SAXS may be due either to dense particles in a low density environment or to pores – or low density inclusions – in a continuous high electron density medium. Therefore, in this work we will use the word "heterogeneity" to design the scattering objects which may be pores or particles.

Morphology was studied using a scanning electron microscope (SEM) Philips XL-30 and specific surface areas were obtained by nitrogen adsorption through the BET method with a surface area analyzer Micromeritics Gemini 2360. In order to give a coherent picture of the most important characteristics the surface fractal dimension was also determined from the nitrogen adsorption isotherms according to the equation proposed by Pfeifer and Cole [28]:

$$\ln\left(\frac{V}{V_m}\right) = \frac{\text{constant} + (D-3)}{3\,\{\ln[\ln(p_0/p)]\}} \quad (1)$$

this equation relates the multilayer coverage of the surface to the relative pressure, p_0/p, where V is the adsorbed gas volume and V_m is the monolayer volume both at standard temperature and pressure; p is the equilibrium pressure and p_0 is the saturation pressure. If $\ln(V/V_m)$ is plotted as a function of $\ln[\ln(p_0/p)]$, a straight line should be obtained whose slope should be proportional to the surface fractal dimension D. This analysis is valid in the range $-2.3 < \ln[\ln(p_0/p)] < 1.1$ [28]. The correlation between the experimental data and the straight line is given by a determination factor R^2.

2.5. Nickel sorption

Batch experiments were carried out at room temperature, mixing in closed vials 0.1 g of each ZnO and 10 mL of $Ni(NO_3)_2$ $6H_2O$ 1×10^{-4} M (10 ppm of Ni^{2+}) solution at pH 5. Samples were stirred for 10 s and shaken for 2 h. The liquids were separated from the solids by centrifugation (5 min at 3000 rpm). Each 5 mL aliquot and their respective patterns were irradiated for 30 min in the Triga Mark III nuclear reactor of the Nuclear Center of Mexico, with a neutron flux of 10^{12}–$10^{13}\ \text{n cm}^{-2}\ \text{s}^{-1}$. The activity of $^{65}Ni^{2+}$ from the 1482 keV peak in each aliquot was measured with an Ortec Ge/hyperpure solid state detector coupled to a multichannel analyzer (4096 channels) previously calibrated with ^{204}Tl (71 keV), ^{22}Na (511 and 1274 keV) and ^{137}Cs (662 keV) radioactive sources and calculated by means of a suitable computer program (Teacher) in the multichannel analyzer.

3. Results

3.1. Compound identification

In Fig. 1, the X-ray diffraction patterns of the samples prepared by combustion and solution combustion techniques are compared to the pattern of the ZnO prepared by calcination of zinc nitrate. The sharp and well-defined peaks, present in all samples, correspond to very crystalline ZnO (zincite). The difference in relative intensities can be interpreted as due to some preferential orientations that may be attributed to variations in crystallite shape. Thus, the crystallite shape of the calcination prepared sample would be different from the one of combustion prepared samples. The infrared spectra did not show any band attributable to organic residues.

3.2. Small angle X-ray scattering (SAXS)

The Kratky plots are shown in Fig. 2. The dried and combustion prepared materials present a lamellar morphology. Still, the slope

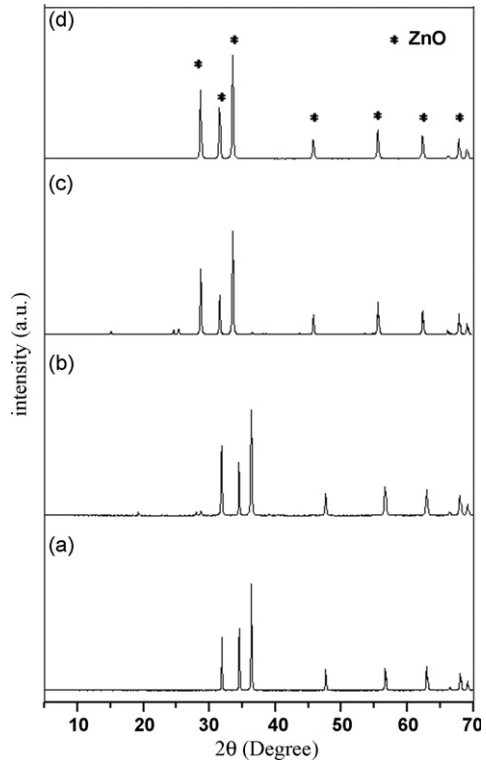

Fig. 1. X-ray diffraction patterns of the samples prepared by (a) calcination of zinc nitrate (sample A_{cal}), (b) by combustion method (sample B_{comb}), (c) by solution combustion with additional 0.5 mL H_2O (sample C_{scomb}), and (d) by solution combustion with additional 1.0 mL H_2O (D_{scomb}).

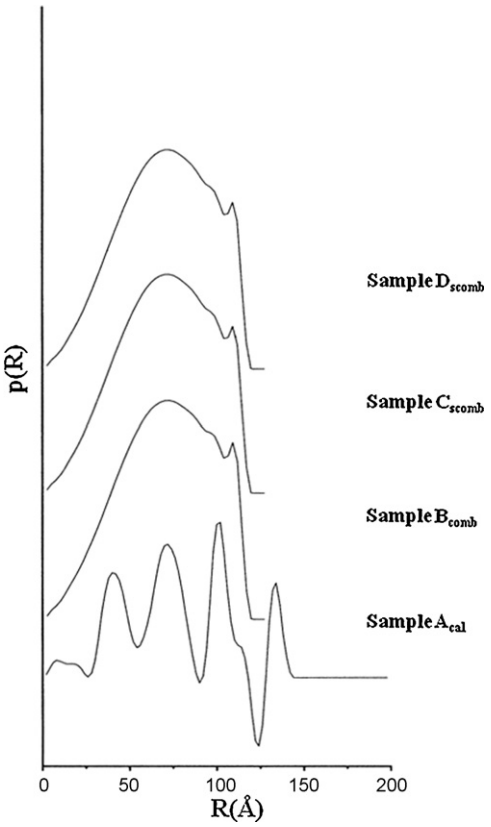

Fig. 3. Particle size distributions determined by SAXS.

of the combustion prepared materials differs from the slope due to the sample prepared by calcination, most probably because the shape of the particles is slightly different. Assuming such morphologies, the heterogeneity size distributions were obtained, Fig. 3. The maxima in the calcined ZnO correspond to radii of 45, 70, 100 and 135 Å, most particles are 100 Å. These values are larger than those obtained for the other prepared materials whose heterogeneity size distributions present a broad peak centered at a radius of 75 Å and a well-resolved peak for a radius of 110 Å.

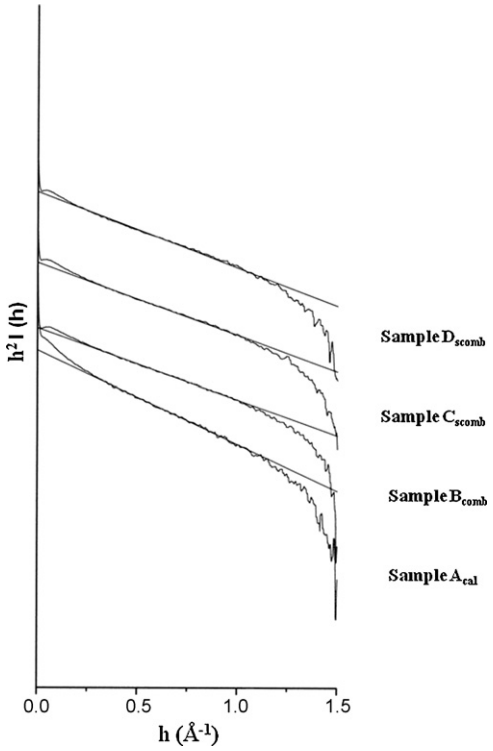

Fig. 2. Kratky plots of prepared samples determined by SAXS.

The fractal dimension, obtained from SAXS experiments, Table 2, follows the same pattern as the highest value, 2.6, was found for the precipitated and calcined sample which does not present a fractal structure. The combustion, sample $B_{(comb)}$, and the solution combustion prepared zincites (samples C_{scomb} and D_{scomb}) are the more fractally structured oxides (2.2). These values are volume fractal dimensions and show that the connectivity of the zincite structure depends on the preparation method. They will be interpreted, in the discussion section, in terms of the surface fractal dimensions obtained by nitrogen adsorption.

3.3. Scanning electron microscopy (SEM)

The size and shape of the grains of the synthesized ZnO determined by SEM are very different (Fig. 4). The particles of the calcined sample A_{cal} are large, irregular, layered and close to 8–20 mμ. Their thickness seems to be *ca.* 0.5–1 μm. The particle surface is smooth and typical of a well-crystallized material.

The combustion prepared ZnO, B_{comb}, presents a porous layered morphology. The thickness of the particles constituted by several very irregular layers seems to be 1 μm, although due to the large number of pores, many particles seem to be filamentous. Open pores of 8 μm are distributed regularly. Small pores, appearing as dot in the micrograph are close to 0.1 μm.

The solution combustion sample prepared with 0.5 mL, sample C_{scomb}, of water seems to be denser as pores have become real craters *ca.* 6–7 μm and the number of very small pores is small. Particles are regular plates *ca.* 5 μm and homogeneous particles whose

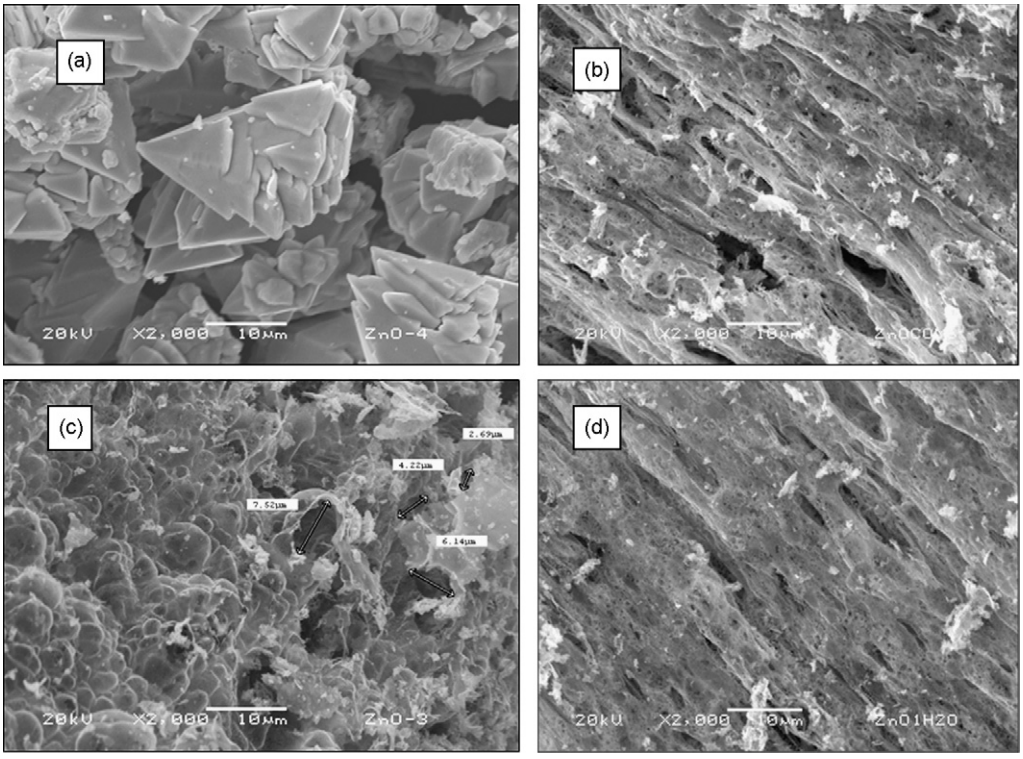

Fig. 4. Top-view SEM images of the ZnO samples. (a) Calcined ZnO (A_{cal}); (b) combustion ZnO (B_{comb}); (c) solution combustion ZnO with additional 0.5 mL H_2O (C_{scomb}); (d) solution combustion ZnO with additional 1.0 mL H_2O (D_{scomb}).

size is close to 0.1 μm. Their external surface is rather smooth.

The combustion prepared material with 1 mL of water, sample D_{scomb}, presents, again, a clear lamellar structure where large ellipsoidal "craters" can be observed, 10 μm × 3 μm. This sample is rather similar to the combustion sample, sample B_{comb}, Fig. 4.

3.4. BET specific surface area

The specific surface area of calcined ZnO (sample A_{cal}) turned out to be 0.6 m^2/g. Instead, all other samples presented areas comprised between 3.6 and 6.1 m^2/g (Table 1). The highest value was 6.1 m^2/g obtained for ZnO 1 mL (sample D_{scomb}). A variation of 0.5 mL of water (from 0.5 to 1 mL) diminishes the surface area in more than 25%, therefore, the control of combustion reaction through water is essential to obtain high specific surface areas. Fig. 5 correlates the specific surface area of ZnO samples obtained by combustion with the water amount added during synthesis.

Table 1
Compounds identified by XRD in each sample and BET specific surface areas.

Sample	Synthesis	Treatment	Compounds	Surface area (m^2/g)
$A_{(cal)}$	Calcined ZnO	Calcination	ZnO (zincite)	0.6
$B_{(comb)}$	Combustion synthesis	Combustion	ZnO (zincite)	3.6
$C_{(scomb)}$	ZnO–H_2O (0.5 mL)	Solution combustion	ZnO (zincite)	4.6
$D_{(scomb)}$	ZnO–H_2O (1 mL)	Solution combustion	ZnO (zincite)	6.1

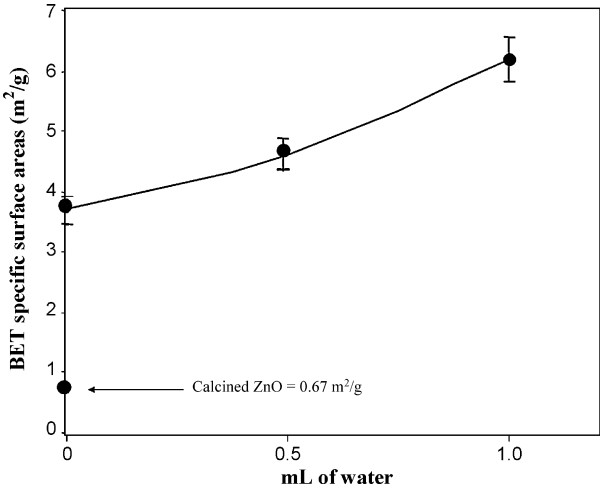

Fig. 5. BET specific surface areas of calcined, combustion and solution combustion prepared samples as a function of additional water amount added during synthesis.

When the surface fractal dimension was obtained from N_2 adsorption data, the values were, for ZnO (sample A_{cal}), 2.0 and 1.9 for sample ZnO prepared by combustion (sample B_{comb}). For both

Table 2
Comparison of the results determined by SAXS, SEM and BET.

Sample	Shape of heterogeneities (SAXS)	Fractal dimension (SAXS)	Pore size distribution, maxima in Å (SAXS)	Particle morphology (SAXS)	Surface fractal dimension (BET) R^2
$A_{(cal)}$	Spheres	2.6	45, 70, 100	No defined morphology	2.1 (R^2 = 0.9622)
$B_{(comb)}$	Lamellae	2.2	Broad, 70	Homogeneous, small particles (*ca.* 0.1 (m)	1.9 (R^2 = 0.9622)
$C_{(scomb)}$	Lamellae	2.2	Broad, 70	Large bubbles, lamellar	1.8 (R^2 = 0.9980)
$D_{(scomb)}$	Lamellae	2.2	Broad, 70	Bubbles, slightly more compact, lamellar	1.8 (R^2 = 0.9526)

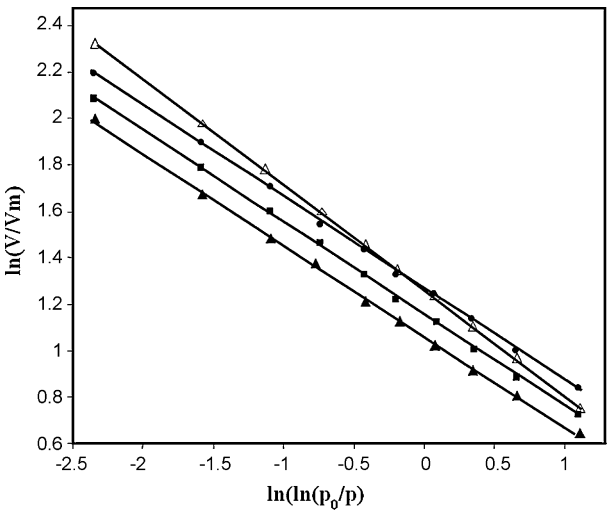

Fig. 6. $\ln(V/V_m)$ versus $\ln[\ln(p_0/p)]$ to determine the surface fractality: A_{cal} (open triangles $R^2 = 0.9622$), B_{comb} (closed circles, $R^2 = 0.9622$), C_{scomb} (closed charts, $R^2 = 0.9980$), D_{scomb} (closed triangles, $R^2 = 0.9526$).

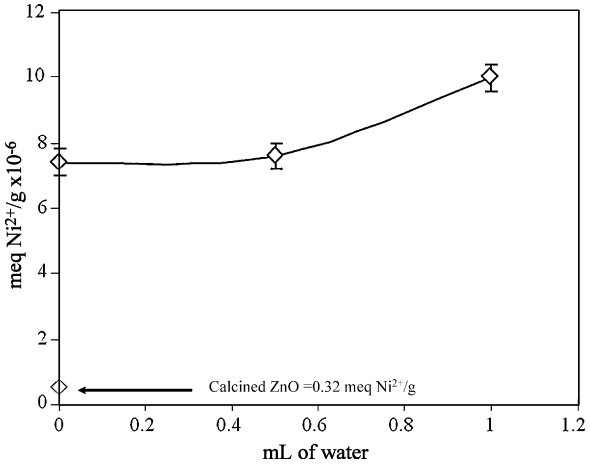

Fig. 7. Ni^{2+} sorption on the combustion and solution combustion prepared samples. Experimental conditions: concentration of $Ni^{2+} = 1.0 \times 10^{-4}$ M; pH 5.5; room temperature.

solution combustion samples, C_{scomb} and D_{scomb}, the surface fractal dimension was 1.8, Table 2 and Fig. 6.

3.5. Nickel retention

The amount of retained nickel (II) ions is shown in Fig. 7. The value for sample A_{cal} was 3.2×10^{-7} meq Ni^{2+}/g, but, for sample $B_{(comb)}$, it was 7.4×10^{-6} meq Ni^{2+}/g and for sample C_{scomb} it was 7.6×10^{-6} meq Ni^{2+}/g and finally for sample D_{scomb}, the value increased up to 1×10^{-5} meq Ni^{2+}/g.

4. Discussion

Our results may be summarized as follows. Specific surface areas were very small. As in X-ray diffraction the peaks are very sharp and well defined the crystallites of ZnO constituting all samples must be larger than 500 Å. Therefore, SAXS curves are due to pores and not particles as the measured sizes are 50–150 Å. Such interpretation is confirmed by the scanning electron micrographs where the observed layered particles present a high amount of holes, showing a clear interlayer connected porosity. Note that although the nickel retention is very high in the D_{scomb} sample, the morphological features of this material are rather similar to those of the other samples, mainly the B_{comb} sample; only the fractal dimension (volume or surface) and the specific surface area vary.

Hence, a clear picture of the prepared materials emerges. The conventionally prepared ZnO, through calcination, sample A_{cal}, has a low surface area and it is not prone to retain nickel. This material reproduces the already reported ZnO in bibliography. The micrographs of solution combustion samples show clear bubbles that explode forming craters and cavities on the surface. Such morphology reveals the presence of vapors that are liberated when the sample is viscous. In this sense, the fractal dimension values determined by SAXS are relevant as they show that those materials (C_{scomb} and D_{scomb}) are fractally structured most probably because of the rapid expulsion of gases.

The combustion prepared ZnO samples, depending on the amount of water, present, then, textural and morphological differences that may be correlated with their nickel retention. Still, they are all well-crystallized ZnO. Given the very small surface area, nickel is most probably retained in the external surface of the particles and a small improvement in that surface is most effective. Hence, a high amount of additional water in the combustion preparation of ZnO is recommended. Indeed, the higher is the amount of additional water, the higher are the specific surface and nickel retention. Such observation is independent of particle shape as sample D_{scomb} prepared with the higher amount of water is morphologically similar to sample B_{comb} which was prepared without water. The difference is fractal dimension which shows that, on the one hand, the pore fractal internal surface, down to molecular scale, promotes a Knudsen diffusion rather than bulk molecular diffusion. Hence, as nickel collides more often with the pore walls it has more probability to be adsorbed. On the other hand, most probably due to fractal surface structure, oxygen atoms of the ZnO structure are more exposed, than local sites of negative charge appear which may adsorb nickel cations.

5. Conclusion

Zinc oxide powders can be easily synthesized by a combustion reaction in a short time using urea. A pure ZnO (zincite) phase was obtained by this simple process. Zinc oxide prepared by combustion method with urea presents a surface area of 3.6 m^2/g, this value is six times higher than that obtained by calcination (0.6 m^2/g). The effect of incorporating additional water in the combustion synthesis of ZnO, *i.e.* the combustion solution method, provides materials with higher surface area, 4.6–6.1 m^2/g, and a higher capacity to retain Ni^{2+}. The sample prepared by combustion with 1 mL of water retained the highest Ni^{2+} amount (1×10^{-5} meq Ni^{2+}/g).

Ni^{2+} adsorption is correlated linearly with surface and volume fractal dimensions determined by BET and SAXS. Morphology depends on the amount of incorporated water, a lamellar structure and large "craters" can be observed. Hence, the material prepared by solution combustion with additional 1 mL of water (surface area: 6.1 m^2/g, surface fractal dimension: 1.8, morphology: lamellar, pore size distribution: broad and centered in 70 Å) presented the best performance in Ni^{2+} retention. Most probably, as more water is added, a fraction of the combustion heat is used to evaporate the water excess as shown by the craters observed in the SEM micrographs. Therefore the active sites in the surface are increased, thus, retaining more nickel ions.

Acknowledgements

The authors tank M. Villa-Tomasa and C. Rodriguez F. from ININ for technical assistance.

References

[1] A. Bunde, S. Havlin, Fractals in science, Springer-Verlag, Berlin, Germany, 1994.
[2] D. Avnir, D. Farin, P. Pfeifer, A discussion of some aspects of surface fractality and of its determination, New J. Chem. 16 (1992) 439–449.
[3] A.V. Neimark, Determination of the surface fractal dimensionality from the results of an adsorption experiment, Russ. J. Phys. Chem. 64 (1990) 2593–2605.
[4] D.A. Ward, E.I. Ko, One-step synthesis and characterization of zirconia-sulfate aerogels as solid superacids, J. Catal. 150 (1994) 18–33.
[5] J. Li, Y. Pan, C. Xiang, Q. Ge, J. Gou, Low temperature synthesis of ultrafine α-Al_2O_3 powder by a simple aqueous sol–gel process, Ceram. Int. 32 (2006) 587–591.
[6] K.C. Patil, S.T. Aruna, T. Mimani, Combustion synthesis: an update, Solid State Mat. Sci. 6 (2002) 507–512.
[7] L.W. Zhong, Zinc oxide nanostructures: growth, properties and applications, J. Phys. Condens. Mat. 16 (2004) 829–858.
[8] E. Tang, B. Tian, E. Zheng, C. Fu, G. Cheng, Preparation of zinc oxide nanoparticles via uniform precipitation method and its surface modification by methacryloxypropyltrimethoxysilane, Chem. Eng. Commun. 195 (2008) 479–491.
[9] K. Zhang, Y. Zhao, F. He, D. Liu, Piezoelectricity of ZnO films prepared by Sol–gel method, Chin. J. Phys. 20 (2007) 721–726.
[10] M. Jayalakshmi, M. Palaniappa, K. Balasubramanian, Single step solution combustion synthesis of ZnO/carbon composite and its electrochemical characterization for supercapacitor application, Int. J. Electrochem. Sci. 3 (2008) 96–103.
[11] H. Chy-Ching, W. Tsung-Yung, Combustion synthesis of nanocrystalline ZnO powders using zinc nitrate and glycine as reactants-influence of reactant composition, J. Mater. Sci. 39 (2004) 6111–6115.
[12] Hwang, Synthesis and characterization of nanocrystalline ZnO powders by a novel combustion synthesis method, Mat. Sci. Eng. B 111 (2004) 197–206.
[13] J.J. Kingley, K.C. Patil, A novel combustion process for the synthesis of fine particle a-alumina and related oxide materials, Mat. Lett. 6 (1988) 427–432.
[14] T. Mimani, K.C. Patil, Solution combustion synthesis of nanoscale oxides and their composites, Mater. Phys. Mech. 4 (2001) 4134–4137.
[15] F. Granados-Correa, J. Bonifacio-Martínez, V.H. Lara, P. Bosch, S. Bulbulian, Cobalt sorption properties of MgO prepared by solution combustion, Appl. Surf. Sci. 254 (2008) 4688–4694.
[16] P. Dieudonne, J. Phalippou, Textural properties of densified aerogels, J. Sol–Gel Sci. Technol. 14 (1999) 249–256.
[17] E. Vinogradova, A. Moreno, V.H. Lara, P. Bosch, Multi-fractal imaging and structural investigation of silica hydrogels and aerogels, Silicon Chem. 2 (2003) 247–254.
[18] J.S. Valente, S. Falcon, E. Lima, M.A. Vera, P. Bosch, E. López-Salinas, Phosphating alumina: a way to tailor its surface properties, Micropor. Mesopor. Mat. 94 (2006) 277–282.
[19] Z. Aksu, Determination of the equilibrium, kinetics and thermodynamic parameters of the batch biosorption of nickel (II) ions onto Chlorella vulgaris, Process Biochem. 38 (2002) 89–99.
[20] J. Severa, B. Jaromir, Handbook of Radioactive Contamination and Decontamination, Elsevier, Amsterdam, 1991.
[21] H. Parab, S. Joshi, N. Shenoy, A. Lali, U.S. Sarma, M. Sudersanam, Determination of kinetic and equilibrium parameters of the batch adsorption of Co(II), Cr(III) and Ni(II) onto coir pith, Process Biochem. 41 (2006) 609–615.
[22] P.N. Pathak, G.R. Choppin, Nickel (II) sorption on hydrous silica: a kinetic and thermodynamic study, J. Radioanal. Nucl. Chem. 268 (2006) 467–473.
[23] O. Glatter, Comparison of two different methods for direct structure analysis from small-angle scattering data, J. Appl. Crystallogr. 21 (1988) 886–890.
[24] O. Glatter, K. Gruber, Indirect transformation in reciprocal space: desmearing of small-angle scattering data from partially ordered systems, J. Appl. Crystallogr. 26 (1993) 512–518.
[25] M. Kataoka, J.M. Flanagan, F. Tokunaga, D.M. Engelman, Use of X-ray solution scattering for protein folding study, in: B. Chanse, J. Deisenhofer, S. Ebashi, D.T. Goodhead, H.E. Huxley (Eds.), In Synchrotron Radiation in the Biosciences, 4, Clarendon Press, Oxford, U.K, 1994, pp. 87–89.
[26] A. Harrison, Fractals in chemistry, Oxford University Press Inc., New York, U.S.A, 1995.
[27] J.E. Martin, A.J. Hurd, Scattering from fractals, J. Appl. Crystallogr. 20 (1987) 61–78.
[28] P. Pfeifer, M.W. Cole, Fractals in surface science: Scattering and thermodynamics of adsorbed films II, New J. Phys. 14 (1990) 221–232.